A Numerical Model of the Ventilated Thermocline

MICHAEL D. COX AND KIRK BRYAN

Geophysical Fluid Dynamics Laboratory/NOAA, Princeton University, Princeton, NJ 08542

(Manuscript received 14 July 1983, in final form 1 February 1984)

ABSTRACT

A steady state numerical solution is found for an idealized, rectangular ocean basin driven by wind and surface buoyancy flux. A three-dimensional primitive equation model is used. In agreement with recent analytical modeling, the thermocline in the numerical solution consists of three regions, quite distinct in their ventilation characteristics. Forming the greater part of the subtropical thermocline is an unventilated "pool" zone located in the core of the subtropical gyre, and a "ventilated" zone to the east. The unventilated "shadow" zone lies farther east and toward the equator. Analysis of potential vorticity on constant density surfaces is used to study the structure of the thermocline. A small but intense zone of convection located in the western boundary outflow, caused by rapid heat loss to the atmosphere, produces source water for the ventilated zone. This water of extremely low potential vorticity (mode water), is distributed widely into the subtropical thermocline. The pool zone forms equatorward of the convective influence, although lateral mixing in the western boundary current provides indirect ventilation within this region. Trajectory analysis is used to illustrate the effects of the individual terms in the density equation on potential vorticity.

1. Introduction

A series of papers has recently been published which addresses the question of the maintenance of the thermocline within the subtropical ocean, utilizing the abbreviated form of potential vorticity, $q = -f\rho_z$, as an analytical tool. Among these is the study by Rhines and Young (1982) where the flow within a stratified wind-driven ocean gyre is modeled in terms of q. Assuming homogenization of q on closed trajectories along isopycnal surfaces, it is found that only small vertical transfers of momentum from the surface (by eddy form drag) are needed to generate the deep gyres found in the western subtropical oceans. McDowell *et al.* (1982) substantiate the theory with data from the North Atlantic in which q is quite homogeneous over large regions on certain density surfaces. Holland *et al.* (1984) extend the observational support to the North Pacific and include results from the unventilated, quasi-geostrophic numerical model exhibiting virtually total homogenization of potential vorticity within the interior thermocline. Ierley and Young (1983) have pointed out that the formal conditions for applicability of the Prandtl-Batchelor theorem, upon which the Rhines and Young theory is based, are not satisfied within a western boundary current with strong mixing. However, Rhines (personal communication, 1983) has pointed out that a moderate mixing in the western boundary current may actually serve to speed up the homogenization of q on adjacent closed trajectories.

The cross-streamline determination of q for closed trajectories which forms the basis of the Rhines and Young theory is supplemented by the model of Luyten *et al.* (1983) (hereafter, LPS) where q is determined directly by flow along streamlines emanating from outcropping zones. This "ventilated" region depends on surface density forcing not present in the former model. The thermocline is characterized as consisting of three zones: a ventilated zone, an unventilated "pool" zone to the northwest, and a "shadow" zone to the south. Within the ventilated zone, the shape of the thermocline at a given density surface, given by q, is dictated by the q of the water at the outcrop region of the density surface, since there is direct (essentially inviscid) advection from the outcrop to the ventilated region. No such advective link exists for the two unventilated zones. The q of the water at the outcrop, must be prescribed in this model. The pool zone corresponds to the flow considered in Rhines and Young, exhibiting closed trajectories on isopycnals. Although the expectation is that such a zone would not be ventilated well, Sarmiento (1983) points out that North Atlantic tritium data show little apparent difference in ages between the ventilated zone and the pool zone. A question arises as to how the pool zone is linked to the ocean surface.

McCartney (1982) has investigated the occurrences of low q (mode) waters in subtropical recirculation zones and found them to be of both subtropical (18°-water) and subpolar origin. The latter are found both to the east, at midpycnocline, and within the Deep Western Boundary Current. In both cases, winter convection producing low q water, and subsequent equatorward advection along isopycnals within the recirculation, are credited for the occurrence of the mode waters.

The purpose of this study is to generate a simple box-ocean numerical solution possessing the gross features of the subtropical thermocline, and analyze it in the terms of the studies cited. Such a model will extend the scope of the LPS model by predicting the production and destruction of q on a basin-wide scale. Clearly, if q at the outcrops is critical in determining the shape of the thermocline, then it is important to know how q is established there. The ability of the present numerical model to incorporate convective processes is critical in this regard if McCartney's scenario is correct. Bryan and Cox (1968) and Holland (1971) have found solutions using models similar to the one used here. The higher speed computers available now have made it possible to improve upon these studies by increasing the grid point resolution and decreasing mixing coefficients. Interpretation of the solution in terms of potential vorticity is a further addition of the present work to the former studies. After a description of the model in Section 2, solutions with and without wind driving are presented in Section 3 in terms of circulation patterns and density structure. The solutions are analyzed in terms of potential vorticity in Section 4, and trajectory analysis is used to trace water mass origins in Section 5. Local balances of density and potential vorticity are also presented along the trajectories. In Section 6 there is a discussion of the sensitivity of the model to the important parameters and a summary and conclusions are stated in Section 7.

2. Description of the model

The model used in this study is the multilevel numerical model described in Bryan (1969). The continuous equations will be given here. A detailed description of the finite difference formulation may be found in the earlier work. The equations of motion are the Navier-Stokes equations modified by the Boussinesq approximation and the hydrostatic assumption. Molecular viscosity is replaced by a term of Laplacian form. Let $m = \sec\phi$, $n = \sin\phi$, $u = a\dot{\lambda}m^{-1}$ and $v = a\dot{\phi}$, where a is the radius of the earth, ϕ the latitude and λ longitude. It is convenient to define the advection operator

$$\mathcal{L}(\mu) = ma^{-1}[(u\mu)_\lambda + (v\mu m^{-1})_\phi] + (w\mu)_z. \quad (1)$$

The equations of motion on a sphere are

$$u_t + \mathcal{L}(u) - 2\Omega nv = -ma^{-1}\left(\frac{P}{\rho_0}\right)_\lambda + F^\lambda, \quad (2)$$

$$v_t + \mathcal{L}(v) + 2\Omega nu = -a^{-1}\left(\frac{P}{\rho_0}\right)_\phi + F^\phi, \quad (3)$$

$$\mathcal{L}(1) = 0, \quad (4)$$

$$g\rho = -P_z, \quad (5)$$

where ρ_0 is unity in cgs units. The conservation equation for the single state variable σ is

$$\sigma_t + \mathcal{L}(\sigma) = F^\sigma. \quad (6)$$

The equation of state is

$$\rho = 1 + \sigma \times 10^{-3}. \quad (7)$$

The F terms represent the effects of turbulent viscosity and diffusion. Let

$$\nabla^2\mu = m^2\mu_{\lambda\lambda} + m(\mu_\phi m^{-1})_\phi. \quad (8)$$

Then

$$F^\lambda = A_{MV}u_{zz} + (A_{MH}a^{-2})\nabla^2 u, \quad (9)$$

$$F^\phi = A_{MV}v_{zz} + (A_{MH}a^{-2})\nabla^2 v, \quad (10)$$

$$F^\sigma = [(A_{DV}\delta^{-1})\sigma_z]_z + (A_{DH}a^{-2})\nabla^2\sigma, \quad (11)$$

$$\delta = \begin{cases} 1, & \text{if } \sigma_z \leqslant 0 \\ 0, & \text{if } \sigma_z > 0, \end{cases} \quad (12)$$

$$\left.\begin{aligned} w &= 0 \\ A_{DV}\sigma_z &= \gamma(\sigma^* - \sigma) \\ \rho_0 A_{MV}(u_z, v_z) &= \tau_0\tau, 0 \end{aligned}\right\} \text{ at } z = 0, \quad (13)$$

$$u_z = v_z = w = \sigma_z = 0 \quad \text{at} \quad z = -H, \quad (14)$$

where A_{ab} is the mixing coefficient corresponding to

$$a = \begin{cases} M \text{ momentum} \\ D \text{ density,} \end{cases}$$

$$b = \begin{cases} V \text{ vertical} \\ H \text{ horizontal.} \end{cases}$$

Eq. (13) provides surface buoyancy flux proportional to the deviation of the current density from the reference density σ^*. The coefficient γ has units of velocity and is taken to be 3 m day^{-1} in this study. This means that the density of the upper level, of thickness 30 m in the present model, adjusts to σ^* on a time scale of 10 days. Convection is incorporated into the model to insure static stability, by Eq. (12). When, at the end of any time step, any two vertically neighboring density points are found to be statically unstable, they are mixed together completely, as if A_{DV} were infinite. For the cases presented here τ is zonal surface wind stress and τ_0 is 0 and 1.

The region considered in this study is shown in Fig. 1. It is a simple box ocean of width 60 deg extending from the equator to 65°N. Symmetry is imposed as the lateral boundary condition at the equator while both components of velocity and the normal gradient of density vanish at the three walls. The total depth H is 4000 m everywhere. Meridional resolution is 1° and zonal resolution is 1.2° producing equilateral grid boxes at about 35°N. Vertically, there are 15 levels whose interfaces are constant in space and time. They thicken from 30 m at the surface to 730 m at the

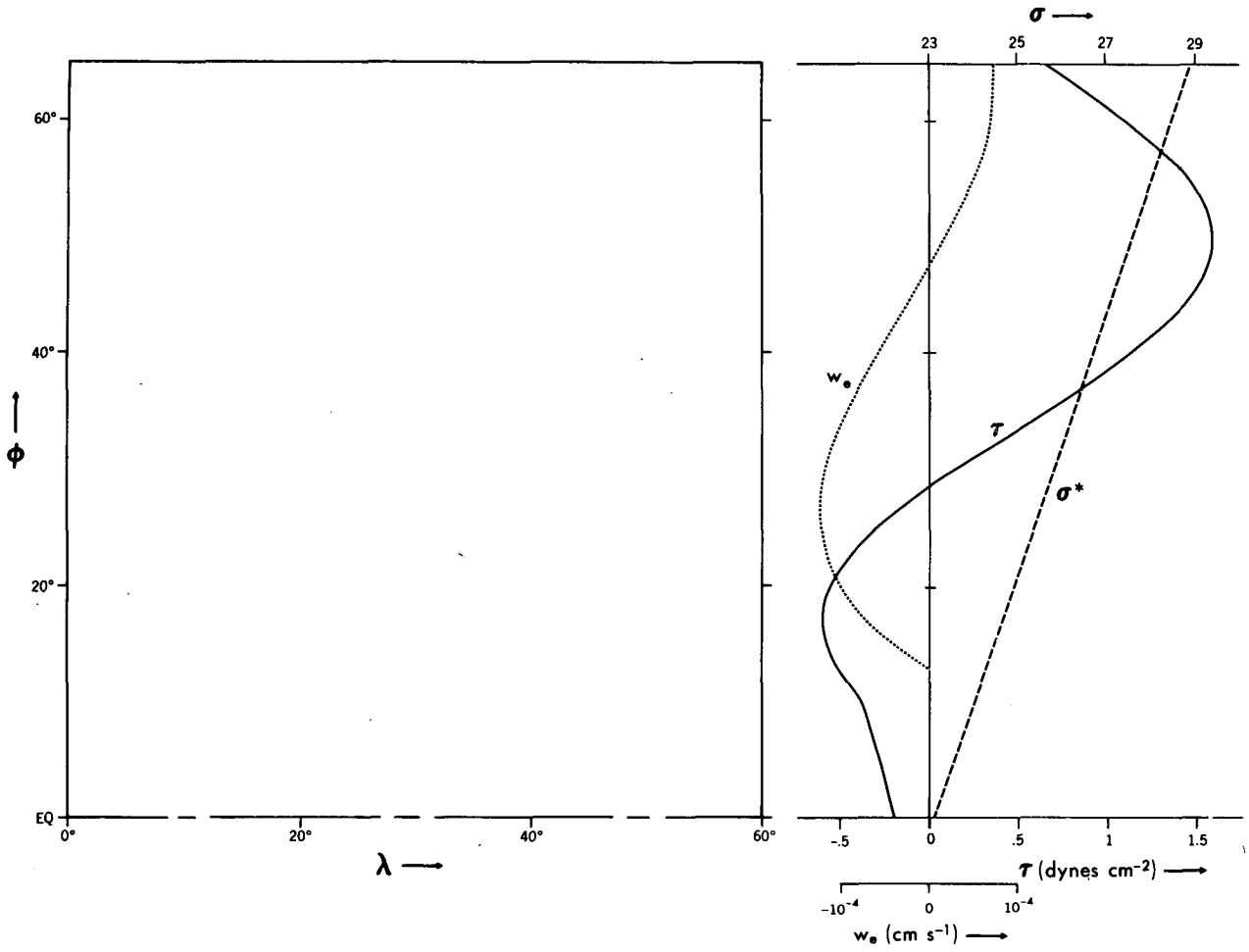

FIG. 1. The basin configuration and surface boundary conditions with the resultant Ekman vertical velocity.

bottom, with six of the levels in the top 400 m. Surface boundary conditions are also shown in Fig. 1. The function τ is based upon long-term, annually and zonally averaged zonal stress over the North Atlantic. The function σ^* is an approximation of average surface density distribution in the North Atlantic. Both are taken to be independent of longitude. The mixing coefficients adopted for this study are $A_{MH} = 10^8$, $A_{DH} = 10^7$, $A_{MV} = 10$, $A_{DV} = 0.3$, all in units of cm^2 s^{-1}.

Due to the extremely long time scales associated with vertical diffusion in the deep ocean it is necessary to integrate several centuries to obtain a steady state solution for a model such as this. At the resolution used here, a time step on the order of 2 h would be necessary, making the integration computationally impractical. However, using the technique of unequal time stepping between momentum and density equations (Bryan, 1984) the computation can be cut by more than an order of magnitude. The steady solution is unaltered by this technique since the terms with local time derivatives vanish. Using this method, steady solutions are obtained in 880 years of integration on the density equation. The mixing coefficients used are just large enough to prevent baroclinic instability so that the solutions are steady at all time scales.

3. Description of the solutions

Two solutions will be described and compared in this study. The first is driven only by surface buoyancy flux. The second is driven by the same surface buoyancy flux, as well as the wind stress shown in Fig. 1. A general description of the circulation and density structure of the two solutions is provided in Figs. 2–5. The pressure at three levels is shown in Fig. 2. Meridional sections of velocity and density averaged over 12° zonal bands along the western boundary, through the center, and along the eastern boundary, are shown in Figs. 3–5. A meridional overturning cell induced by the surface buoyancy flux is apparent in the no-wind case, with rotational effects acting to intensify the meridional component of the cell against the western boundary. The downward component of the cell is intensified against the northern wall. The

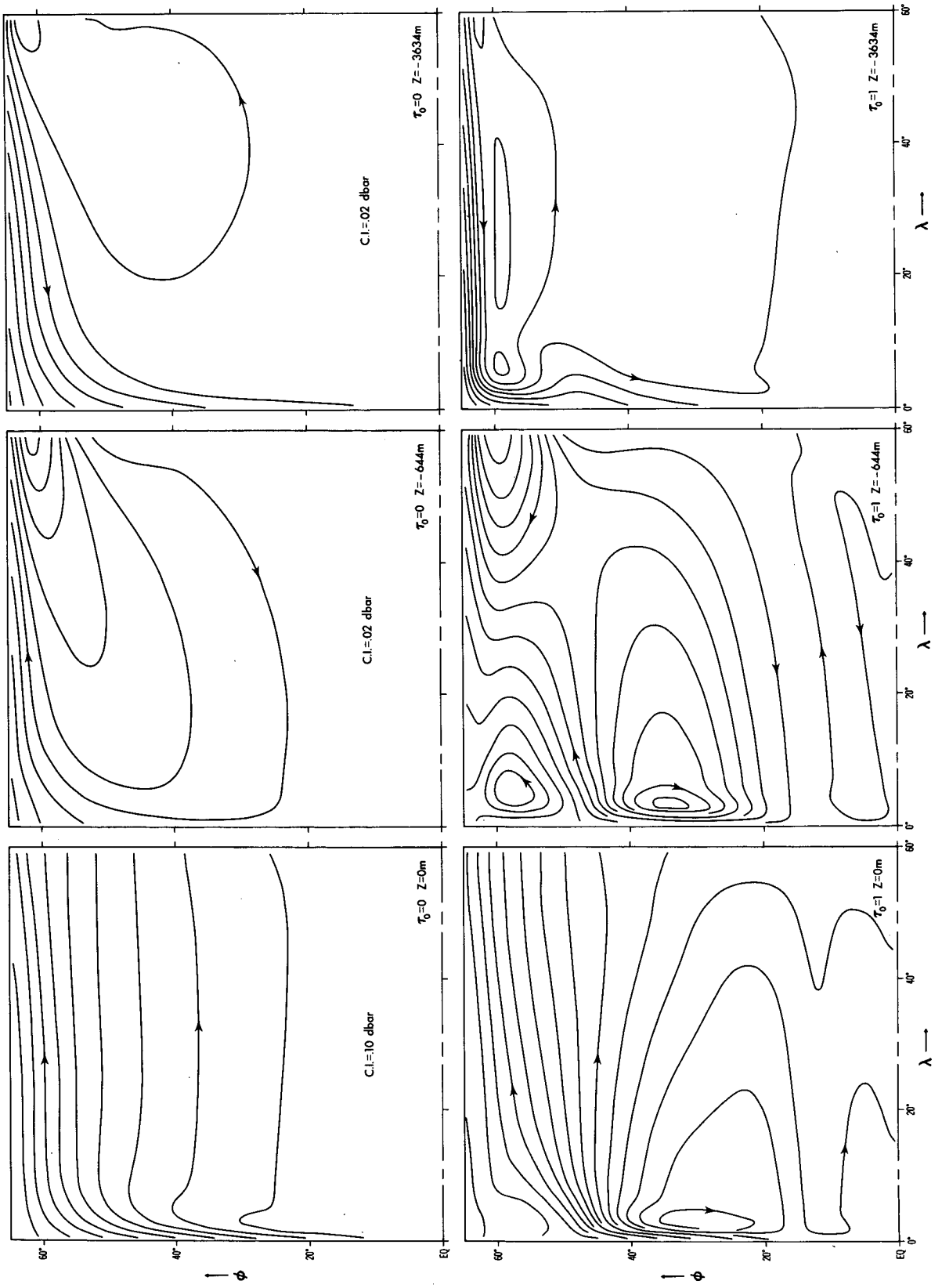

FIG. 2. Pressure at three levels for the case of no wind (above) and the wind-driven case (below).

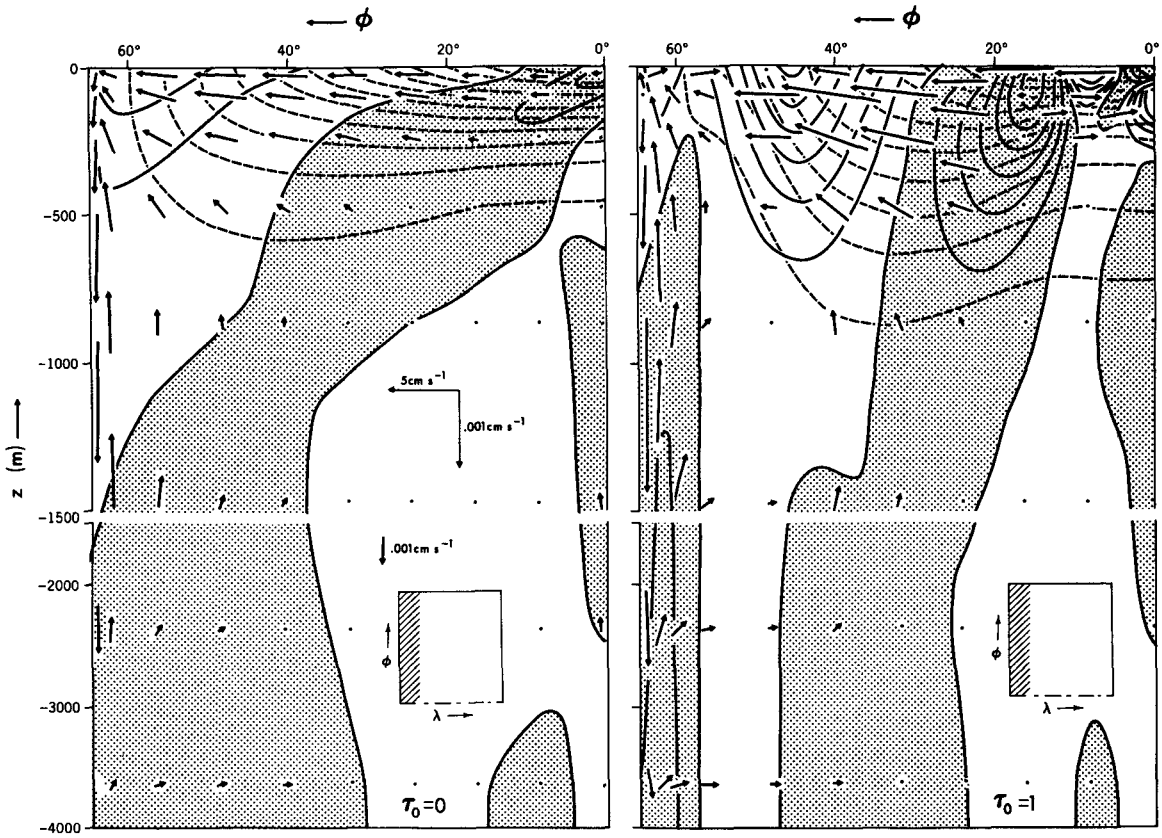

FIG. 3. A meridional section, averaged zonally across the western 12° of the basin (shown by hatching in the inset), for the no wind and wind-driven cases. v and w components of velocity are given by vectors, and u is contoured by solid lines at an interval of 1 cm s^{-1}, with stippling indicating westward flow. Isopycnals are indicated by dashed lines at a 0.4 sigma unit interval.

upward component comprises the broad interior upwelling which maintains the thermocline against vertical mixing. Eastward drift across the basin in the upper ocean, in geostrophic response to the surface boundary condition, drives a zonal overturning cell which deepens with latitude, as evidenced by the downward slope of the zero line in u on Figs. 3–5 as one proceeds from low to high latitudes. Near the northern wall, this cell extends to the bottom, producing a deep westward return flow against the northern wall which then turns southward as the deep component of the meridional cell. The cross-isopycnal vertical motion required along the eastern wall to connect the inflow and outflow there, is balanced in the density conservation equation by mixing processes.

When wind is applied in addition to surface buoyancy forcing, three gyres are formed in the vertically averaged flow, consistent with Sverdrup theory. The pressure patterns at the bottom of Fig. 2 indicate how the model combines the effects of the two driving forces. The subpolar gyre is more barotropic in nature due to the vanishing vertical density gradient. Contours of the u component of momentum in the right-hand panels of Figs. 3 and 4 indicate the vertical structure of the gyres. A South Equatorial Current and Equatorial Undercurrent are formed at the equator.

In the center of the basin (Fig. 4) the vectors indicate the broad southward flow which is consistent with Sverdrup theory within the subtropical gyre. Meridional Ekman surface drift is also indicated. Ekman downwelling produced by convergence of the surface drift is evident by the downward tilt of the southward flow. This flow along isopycnal layers, connecting the surface outcrops with the interior of the thermocline, is the ventilation mechanism of LPS. At the eastern wall (Fig. 5), the wind-driven zonal currents are quite weak (except at the equator), although the southward flow within the subtropical gyre is evident.

The thermocline in the wind-driven case can be seen in Figs. 3–5 to be quite different in shape to that of the no-wind case. To geostrophically support the zonal currents required by the wind, the isopycnals must first penetrate more deeply from their outcrops and then bow upward across the North Equatorial Current. This necessitates a thicker thermocline, bulging downward in subtropical latitudes. Such an effect is produced by the introduction of water of low potential vorticity into the subtropical thermocline. It is

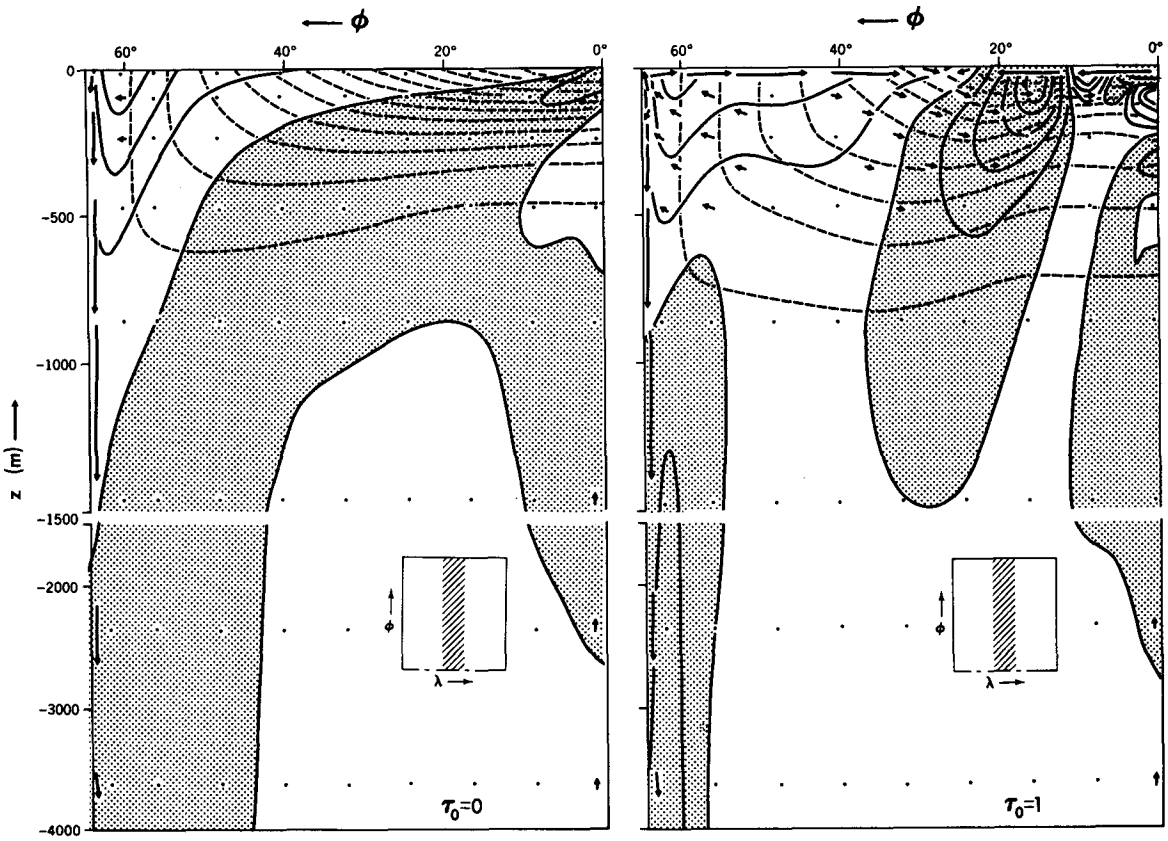

FIG. 4. As in Fig. 3 but for the center 12° of the basin.

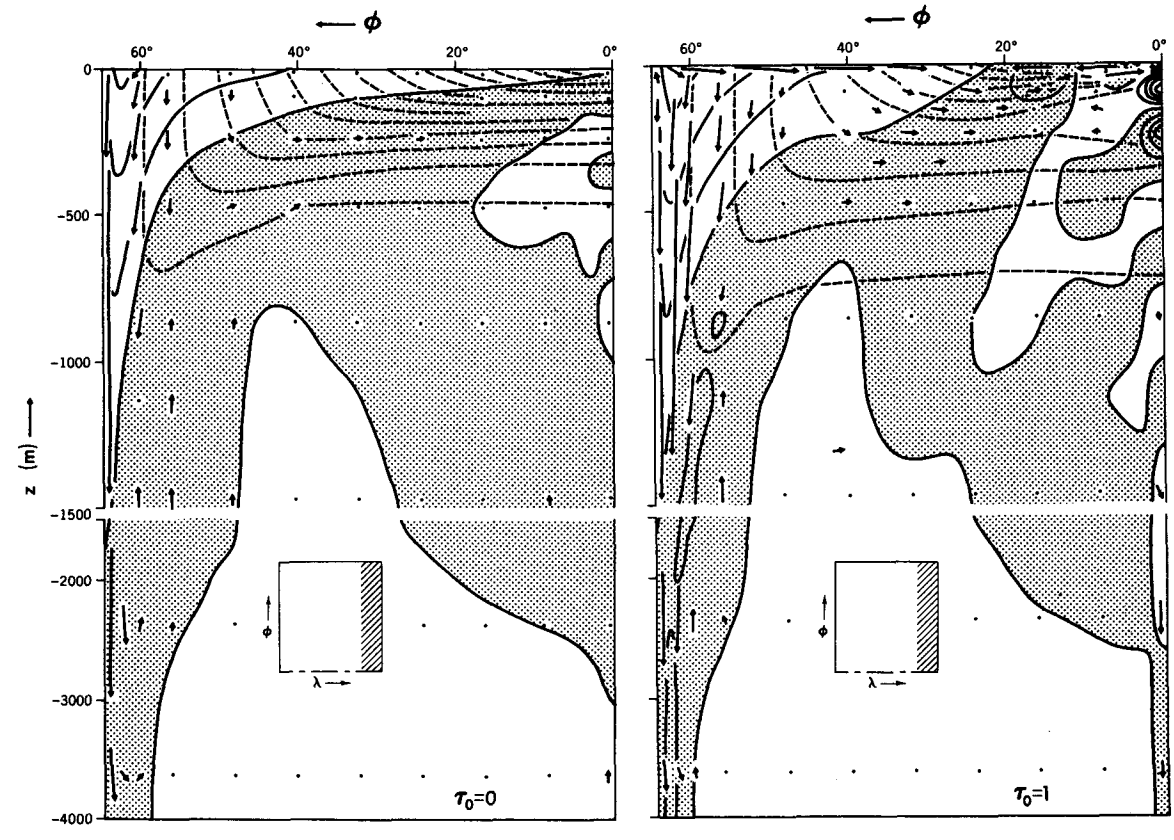

FIG. 5. As in Fig. 3 but for the eastern 12° of the basin.

this process which will be addressed in the remainder of this study.

4. Potential vorticity analysis

A clearer contrast may be seen in the shapes of the thermoclines of the two solutions by considering the abbreviated potential vorticity, $q = -f\sigma_z$. Figs. 6 and 7 show q on a vertical section 25° east of the western boundary for the zero wind and wind-driven cases respectively. The pattern in the zero wind case is relatively simple, with q going to zero at the equator where f vanishes, and at the northern wall and at depth where σ_z vanishes. A maximum forms in the shallow subtropical thermocline. When wind driving is added, the maximum is essentially split in two by an injection of low q water from the north, penetrating into the thermocline. A shallow maximum persists and moves somewhat equatorward while a deeper maximum is formed below the low q tongue. A section observed along 50°W in the North Atlantic is shown in Fig. 8 adapted from McDowell *et al.* (1982). Although the vertical scale is somewhat different due to the shallower thermocline of the model, the shape is similar, showing a minimum (18° water) within the thermocline, underlaid by a maximum. The observations are taken in the fall when the surface q is high due to the seasonal thermocline. Sections of q along 65°W and along the GEOSECS track show the same general features. Although the model produced minimum in q does not penetrate as far equatorward as the observations show, the low q source and a tendency for equatorward penetration is present.

In Fig. 7, three surfaces have been plotted which pass through the features of interest in the q pattern. For purposes of studying the mechanism by which these features arise, contours of q and geostrophic flow lines, are shown along these surfaces in Fig. 9. The flow lines are contours of the Bernoulli function,

$$B(\sigma_0) = P_s + g\int_{z(\sigma_0)}^{0} [\rho - \rho(\sigma_0)]dz, \qquad (15)$$

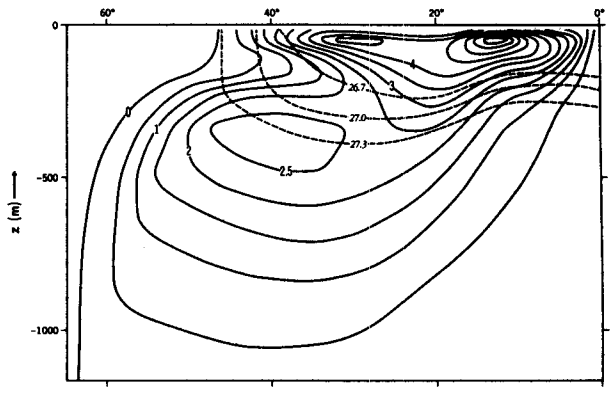

FIG. 7. As in Fig. 6 but for the wind-driven case with three sigma surfaces superimposed.

where σ_0 is the layer in question and P_s is the pressure at the surface of the ocean. The patterns are carried poleward to the point at which their respective surfaces intersect the 95 m isobath (bottom of 3rd model level). In Fig. 9(a) q at 95 m is plotted with the intersections of the three surfaces superimposed. This field represents the advective boundary condition for the surfaces where flow is equatorward at the intersections. At this level, q is zero in a band across the poleward end of the basin due to negative surface buoyancy flux there and the resulting convection. At the western boundary, q is quite high due to the upward turning isotherms. However, as the warm water of the western boundary current moves into colder latitudes, it is affected quite strongly by negative surface buoyancy flux and convection. This results in a pool of low q water in the immediate outflow region and gives the q isolines to the east a southwest to northeast tilt. The effect of convection acting on western boundary currents to produce low q waters has been noted by Gordon (1981). The surface density condition has just the opposite effect on the southward flowing boundary current of the subpolar gyre, producing a large q region. Fig. 10 is redrafted from the atlas of Robinson *et al.* (1979)

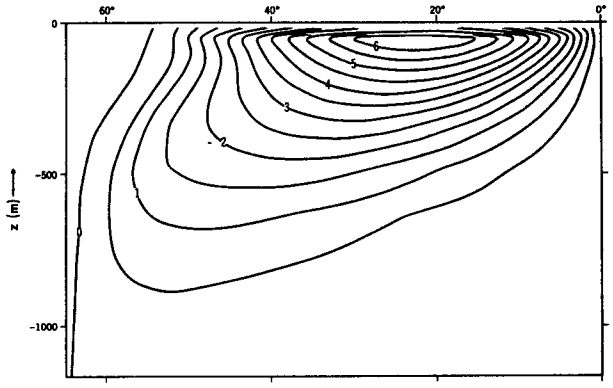

FIG. 6. Potential vorticity ($-f\sigma_z$) at $\lambda = 25°$ for the no wind case in units of 10^{-9} cm^{-1} s^{-1}.

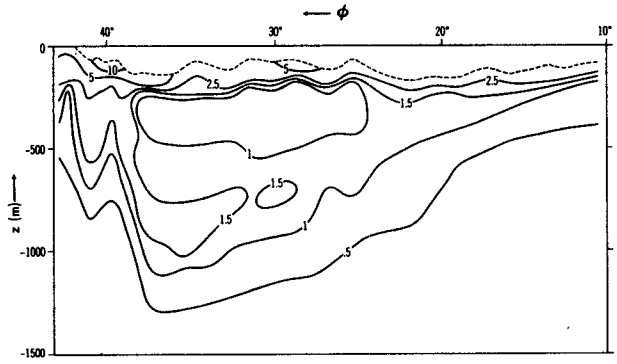

FIG. 8. Potential vorticity ($-f\sigma_z$) at 50°W in the North Atlantic in units of 10^{-9} cm^{-1} s^{-1}, adapted from McDowell *et al.* (1982).

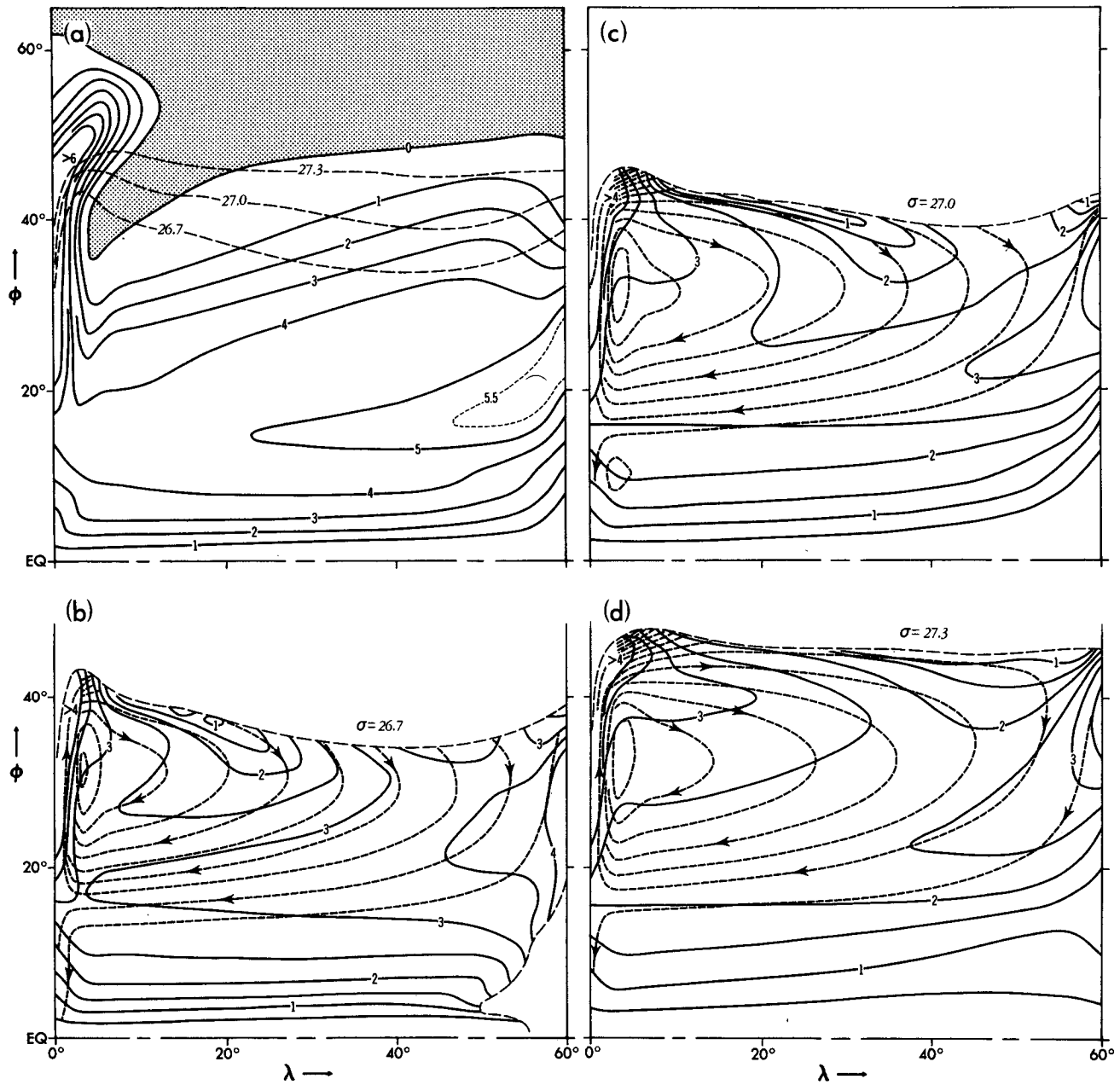

FIG. 9. Potential vorticity ($-f\sigma_z$) at $z = -95$ m (a), and on the 26.7, 27.0 and 27.3 sigma surfaces (b, c, d) in units of 10^{-9} cm^{-1} s^{-1} (solid lines). The Bernoulli function with contour interval 4 cm (equivalent vertical displacement) is shown as short dashed lines in b, c, d. The intersection of the sigma surfaces with $z = -95$ m is shown in long dashed lines.

and shows the depth at which the temperature in the North Atlantic is 1.1°C less than the surface temperature. Data for the month of April is used to show the effects of winter convection. In support of the model solution, a tongue of shallow depths, implying high q water in the upper 100 m, penetrates northeastward from the western boundary, while positioned immediately to the east is a tongue of large depths, implying low q water, penetrating southwestward. At the eastern wall in the model, vertical motion due to surface inflow, dictated by the surface density condition, produces a q maximum.

Each of the three zones discussed by LPS is evident on the density surfaces (Fig. 9b, c, d). These consist of a ventilated zone, fed by flow lines emanating from the outcrop, a pool zone surrounded by closed flow lines, and a shadow zone to the south in which the flow is quite weak. The effect of convection acting on

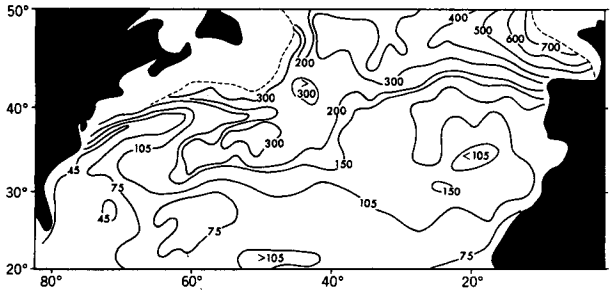

FIG. 10. Depth in meters at which the temperature in the North Atlantic in April is 1.1°C less than the surface temperature, redrafted from the atlas of Robinson *et al.* (1979).

the western boundary current extension is evident where many of the flow lines pass right out of the surfaces as they turn eastward. As σ increases and the corresponding outcrop moves poleward, more of the subtropical gyre is contained within the latitudinal extent of the σ surface. This means the pool zone enlarges and the ventilated zone shrinks. The model of LPS predicts this effect as well. Both advective and diffusive effects are evident in the q patterns. Tongues of high and low q follow flow lines from the sources and sinks at the boundaries, being diminished downstream by the action of diffusion. Due to the angle between the σ surface intersections at 95 m and the isolines of q there, ventilation brings low q, or mode waters into deeper layers at points which are progressively removed from the western boundary. This agrees well with the observations of McCartney (1982) in which mode waters are identified at progressively greater σ surfaces across the Atlantic from west to east.

The origin of the low q tongue penetrating the subtropical thermocline at $\lambda = 25°$ in Fig. 7 can be seen from Fig. 9b and c to be the pool of low q water formed by convection on the western boundary current outflow. The subsurface maximum is seen in Fig. 9d to be the result of eastward subsurface advection of high q waters out from the western boundary while the surface maximum in q emanates from the eastern wall. This source of high q water at the eastern wall is excluded *a priori* from the inviscid model of LPS, since a condition of no normal flow is imposed there in all layers outcropping in the subtropical gyre. An inviscid model cannot absorb inflowing surface waters and allow them to flow out at lower levels. Recently, Pedlosky (1984) has relaxed this constraint in the LPS model.

5. Trajectory analysis

Further understanding of the mechanisms involved in the formation of q within the subtropical thermocline of the model may be obtained by considering water particle trajectories which supply the regions in question. This may be done in the model by starting at a point within the region and using the three-dimensional velocity field generated by the model to integrate the position of the particle backward in time. A trajectory has been plotted in Fig. 11 with an ending point in the center of the ventilated region of the 27.0 surface (Fig. 9c), and in Fig. 12 with an ending point in the pool region of the same surface. The trajectory in Fig. 11, typical of the trajectory of points in the ventilated region, is joined at a point near the surface, within the Ekman drift. (Earlier, the particle had risen from the deep ocean in the upwelling along the western boundary). As it nears the North Equatorial Current it turns westward, sinking at the same time due to Ekman convergence, and is carried to the western boundary. After rising along the western boundary due to upwelling there, the particle turns eastward and resumes its descent into the thermocline. (From point Z the particle reenters the western boundary current at a deeper level than before and exits the subtropical gyre, flowing toward the poleward-eastern corner where it sinks to the deep ocean).

The section of the trajectory for which the density of the particle is less than 0.2 sigma units greater than the density of the ocean surface directly above is designated by hatching. This may be considered the region for which the particle is exposed to surface conditions, or "ventilated." The density of the particle at different points along the trajectory is shown in the middle left panel of Fig. 11. Its flow is nearly isopycnal except within the western boundary current, where it increases in density by a full sigma unit. The lower left panel of Fig. 11 shows the local balance of terms in the density conservation equation [Eqs. (6) and (11)] at each point along the trajectory. "Advection" is the advective term of Eq. (6). "Vertical diffusion" is the first term on the right in Eq. (11) where $\delta = 1$ in Eq. (12). "Convection" is the same term when $\delta = 0$. (In practice, both of these terms can be nonzero at once since vertical diffusion goes on in the presence of convection.) "Horizontal diffusion" is the second term in Eq. (11) and "surface flux" is the change in density due to the surface boundary condition. The local rates of change of density by these terms have been normalized by the time rate of progress of the particle along the abscissa, so that the net effect on the density of the particle is proportional to the area under the curves.

Weak horizontal diffusion acts on the particle in its westward flow, increasing its density slightly. Within the western boundary current, horizontal diffusion mixes the particle with denser particles to the west. As it passes point V, it is mixed strongly by convection with heavier particles from above, created by the surface density condition. Vertical diffusion is active in the eastward component of the trajectory, responding to the discontinuity introduced into the water column by convection. The net increase in density along the trajectory is roughly equally divided between diffusive and convective effects. In the middle right panel q is

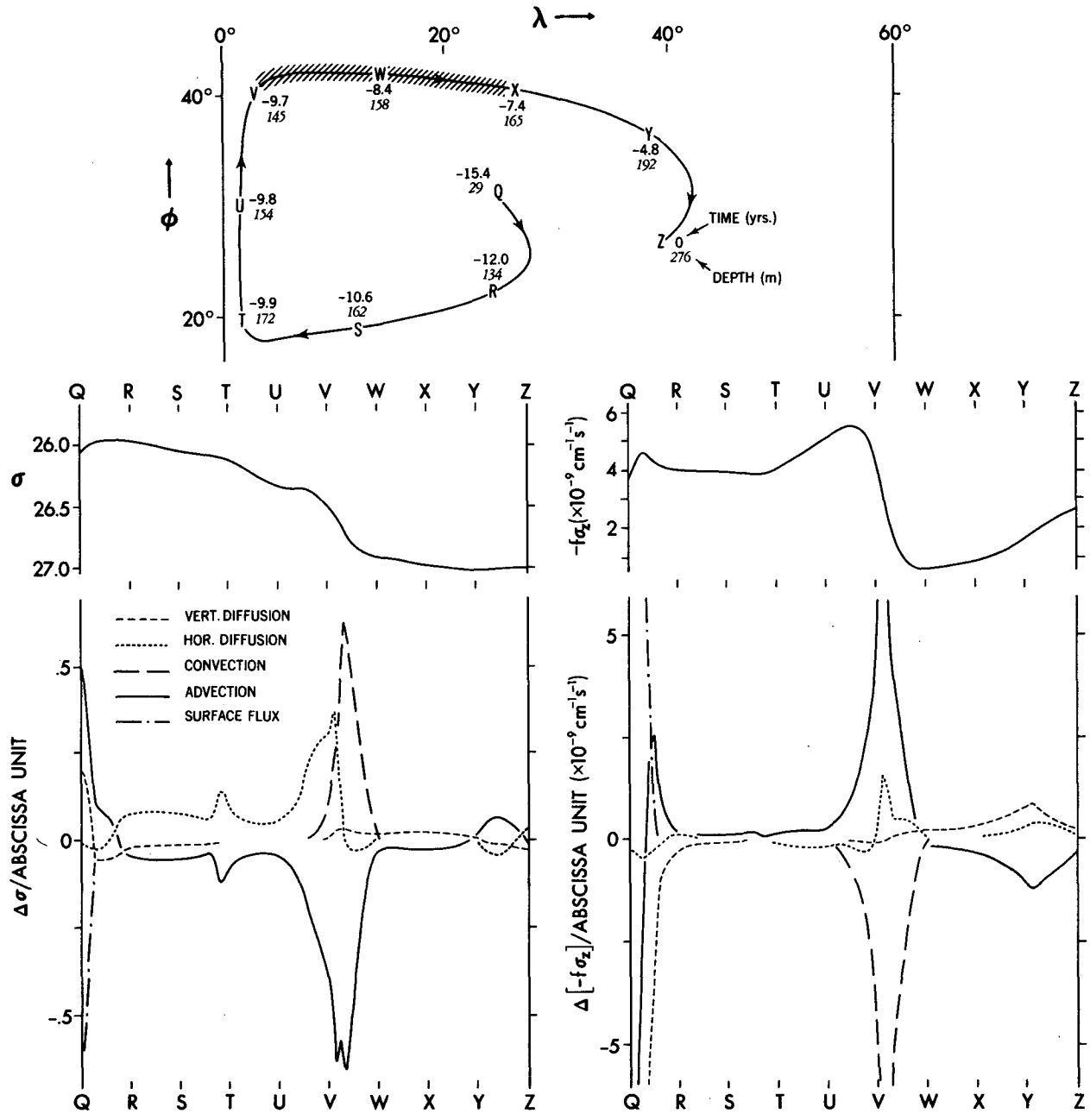

FIG. 11. (Top) A trajectory ending in the ventilated region of the 27.0 sigma surface. Hatching indicates exposure to surface conditions. (Middle) The density and potential vorticity of the particle at points along the trajectory. (Bottom) Effects of the various terms in the density equation on density and potential vorticity at points along the trajectory.

plotted. After leaving the surface layer, it remains relatively constant until reaching the western boundary current where it first increases and then decreases sharply in the outflow region. This is followed by a slow increase in q as the particle enters the interior thermocline. The effect of the individual terms of the density equation on q is shown in the lower right panel. These curves are constructed by taking the vertical derivative of the terms presented on the left and multiplying by $-f$. The peak in q between points U and V is caused by advective effects in the western boundary current. The sharp decline at point V is produced entirely by convection, with advection and horizontal diffusion acting to counter it. The gradual increase in q along the eastward flow is due primarily to vertical diffusion, with horizontal diffusion playing a minor role. Advection of low q water along this part of the trajectory serves to counter the diffusive effects.

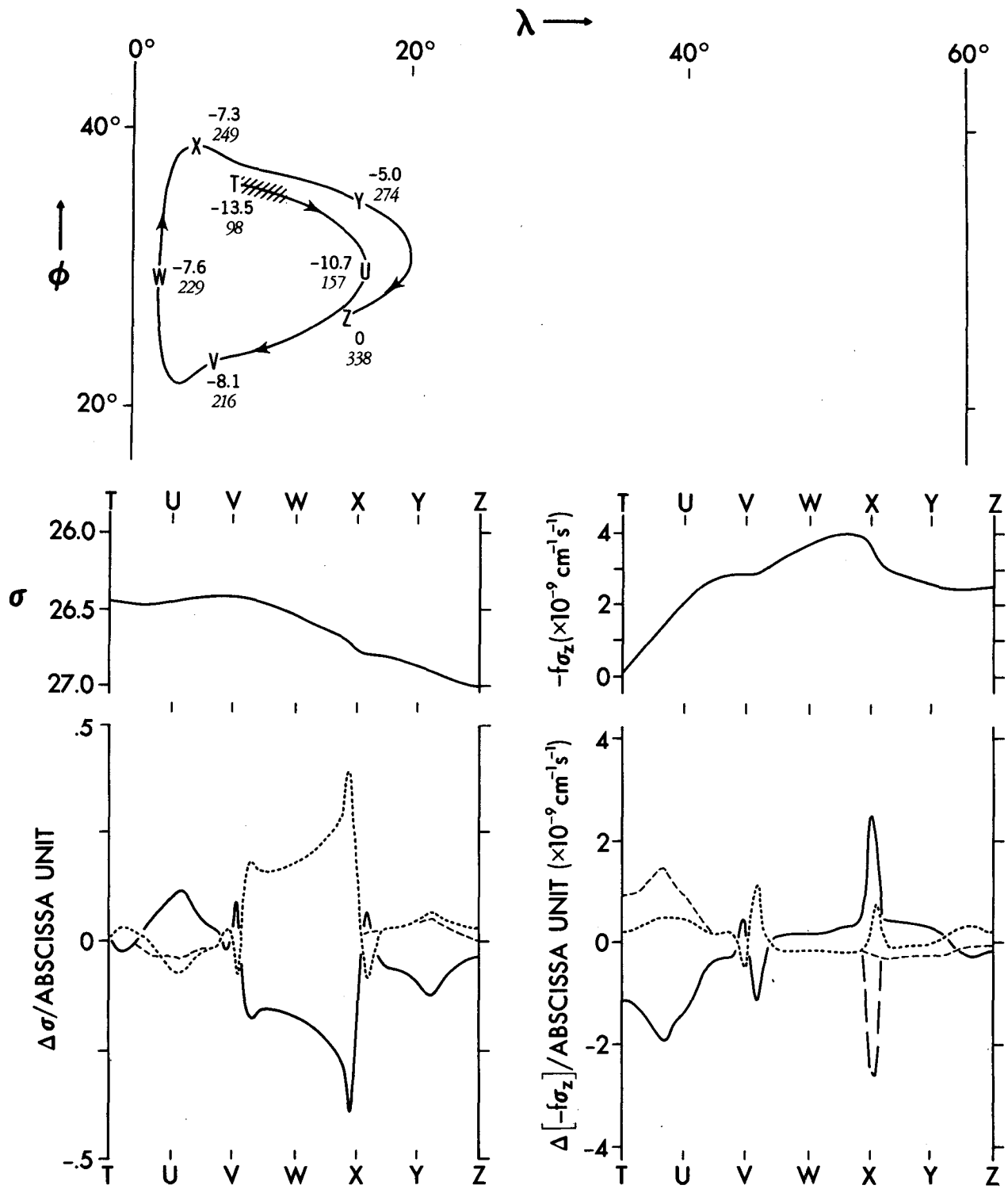

FIG. 12. A trajectory ending in the pool region of the 27.0 sigma surface. (See Fig. 11).

The trajectory of Fig. 12, typical of trajectories within the pool zone, is joined just after the particle turns eastward from the shallow western boundary current. (Earlier, the particle had risen from the deep ocean into the equatorial gyre and had been brought into the shallow subtropical gyre by poleward Ekman drift.) At point T, the particle has just passed through the shallow southern tip of the convection zone indicated

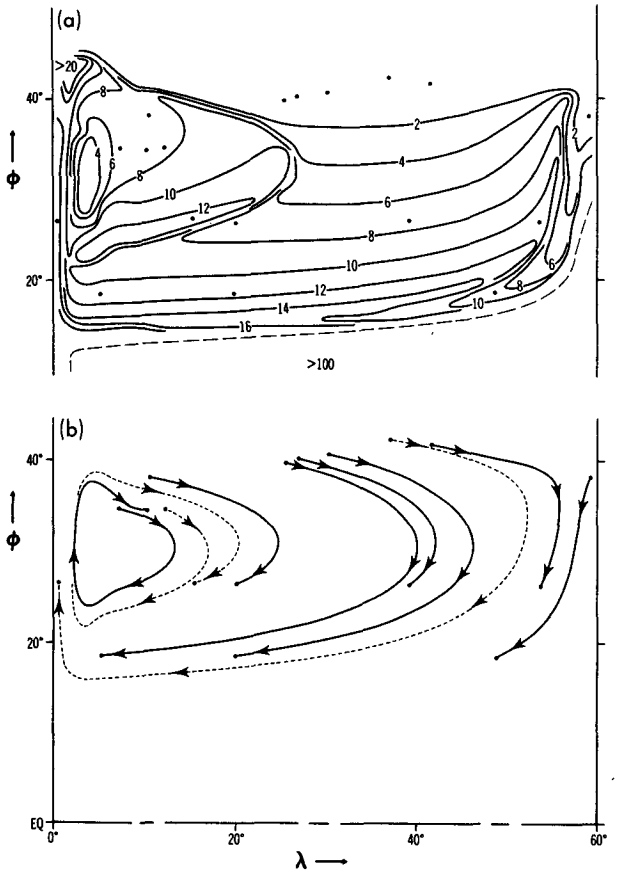

FIG. 13. (a) Advective time since exposure to surface conditions in years. (b) Representative trajectories from the point of exposure to surface conditions. Both diagrams are for the 27.0 sigma surface.

by stippling in Fig. 9a. Its q is near zero and it is ventilated to the surface of the ocean. In these regards it is similar to point W of the previous trajectory. However, its density is still well below the value of the surface (27.0) we are considering. The particle arrives at the 27.0 surface after passing through the western boundary current, where it undergoes an increase in density due to horizontal mixing with denser particles to the west. By this time, the q of the particle has increased considerably and is primarily reflective of the high q of the western boundary current. (From point Z, the particle continues its downward spiral for three additional circuits, then flows from the western boundary current toward the poleward-eastern corner where it sinks to the deep ocean.) Convection at point X penetrates to a point just above the depth of the trajectory. Therefore it does not affect the density of the particle, but does decrease q slightly. The greatly diminished role of convection at this point compared to point V of the previous trajectory is the primary reason that the pool, or inner trajectories of the subtropical gyre in Fig. 9b–d advect high q water away from the western boundary, whereas the ventilated, or outer trajectories advect low q water away from the western boundary.

Sarmiento (1983) has interpreted tritium observations in the North Atlantic in terms of time scales of exchange from the surface of the ocean. He finds time scales averaged over entire density surfaces of 7–20 years for the upper and middepth subtropical thermocline. By integrating trajectories backward in time as in the previous discussion, advective "age" since ventilation may be calculated for any point in the numerical solution. Fig. 13a depicts the ages in years, of particles on the 27.0 surface. As before, the criterion for ventilation is that the particle be within 0.2 sigma units of the ocean surface. The advective ventilation age is the time taken for the particle to proceed from its last point of ventilation to its present position. A sharp age front separates the directly ventilated region from the pool region (where particles must complete an entire circuit of the gyre before arriving on the 27.0 surface.) This contrast is illustrated in Fig. 13b where several of the trajectories have been plotted. Their ventilation points and ending points are repeated in Fig. 13a. Note that the post-ventilation segments of the trajectories of Figs. 11 and 12 are repeated here. The average age over the subtropical region agrees well with those estimated from observations of tritium. Although the ages are greater in the pool region, they are mostly within a factor of two of the ages in the directly ventilated zone at the same latitude. Near the core of the gyre, where the particles spend a greater proportion of their time under the influence of the mixing in the western boundary current however, the net ventilation time scale of a particle in the pool zone may be quite different from the pure advective time scale. To give an idea of the importance of mixing during the advective ventilation of the 27.0 surface, the net change in density in sigma units, from the beginning to the end of the ventilation trajectories, is

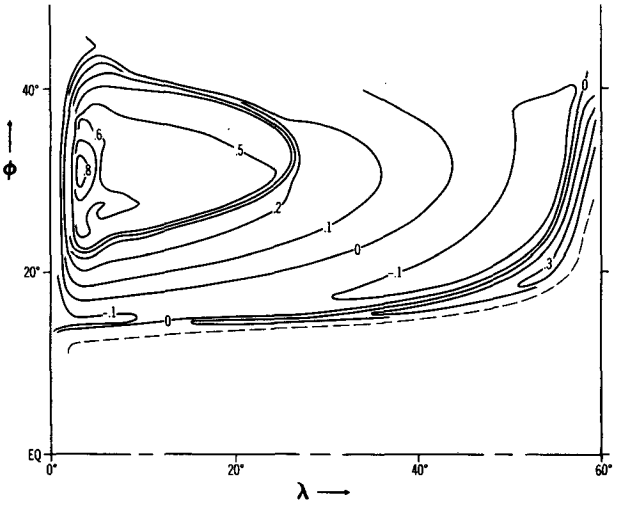

FIG. 14. Change in sigma along the trajectories to σ = 27.0.

shown in Fig. 14. As may be expected, there is a sharp rise in this quantity from the ventilated to the pool zone, reflecting the mixing along the trajectories in the pool zone, primarily within the western boundary current. The post-ventilation segments of the lower left panels of Figs. 11 and 12 support this scenario.

It has been mentioned earlier that the surface buoyancy flux boundary condition produces zonal flow into the eastern wall at the surface. Downwelling occurs at the wall, balanced in the density conservation equation by (primarily) horizontal diffusion. The downwelling produces an additional tongue of short advective ventilation time along the equatorward flank of the subtropical gyre in Fig. 13. The effect of diffusion on these particles is seen in Fig. 14.

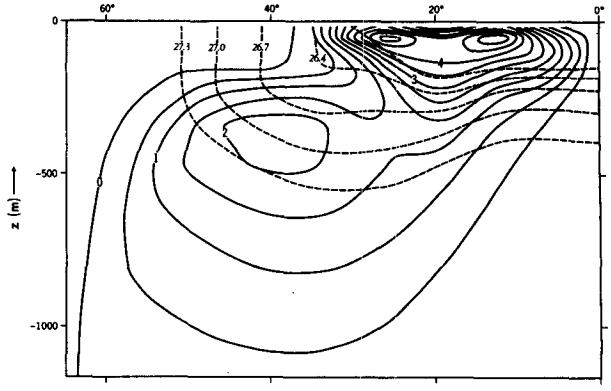

FIG. 15. Potential vorticity ($-f\sigma_z$) at $\lambda = 25°$ for the wind-driven case with $\gamma = 0.3$ m day^{-1}, in units of 10^{-9} cm^{-1} s^{-1}.

6. Model parameter sensitivity

The density and potential vorticity budgets illustrated in Figs. 11 and 12 indicate that nonadvective effects are critical in the formation of the subtropical thermocline in the model. Convection allows water particles to pass laterally across density surfaces, while at the same time reducing their potential vorticity strongly. Diffusive processes also foster cross-isopycnal flow and alter q as well. Quantitative aspects of the model thermocline which are clearly sensitive to the parameters which govern these processes are the size and density of mode water masses, thermocline depth, and relative size of ventilated and pool regions within the subtropical gyre.

Since the diffusive coefficients have been made as small as possible while retaining a time steady solution, the only way to study effects of reducing these coefficients is to use a higher resolution, eddy resolving model. The mixing effects of mesoscale eddies are then included explicitly in the model and the diffusive coefficients can be reduced considerably. Such an experiment is in progress at present and will be reported later.

The parameter affecting convection most directly is γ, the surface restoring coefficient from Eq. (13). Haney (1971) first proposed this formulation for the surface flux of buoyancy, and estimated from the surface heat balance equations and observations that γ should be approximately 0.7 m day^{-1}. The value used in this study, 3 m day^{-1}, provides a more vigorous buoyancy flux through the surface, causing convection to occur more rapidly in areas such as the western boundary current outflow. Since this process is so critical to the formation of low q waters within the subtropical thermocline, an additional experiment has been conducted in which γ is decreased by one order of magnitude to 0.3 m day^{-1}, thereby bracketing the value suggested by Haney. In all other respects the model is the same as that used in the wind-driven case described earlier. The equivalent of Fig. 7 is shown for this case in Fig. 15. The gross features of the potential vorticity cross-section are similar, indicating vigorous ventilation in this case as well. The greatest difference with the previous case is at the surface, poleward of 35° where the low q waters have penetrated further south due to the relaxed surface condition. The region of strong convection in the western boundary current outflow becomes less intense but broader. On a trajectory such as that of Fig. 11, the potential vorticity decreases more gradually as it leaves the western boundary. However, the decrease persists further to the east, eventually resulting in near-zero potential vorticity as in the previous case.

The distribution of σ^* in Eq. 13 would also affect the convective production of low q waters. McCartney *et al.* (1980) report anomalously large masses of mode waters in the North Atlantic following the severe winter of 1976–77. The present model could be used to study such transients by temporarily increasing the value of σ^* to simulate increased cooling during a severe winter. The results of the present experiments indicate that the mode water signature so produced might be evident for several years following, as it proceeds into the interior of the subtropical gyre.

7. Summary and conclusions

Many features of the ocean circulation model presented here are not essentially different from models studied earlier. It has a uniform depth and simple geometry, and the parameter range is too viscous and diffusive to allow mesoscale eddies to grow through baroclinic instability. The motivation for revisiting these solutions is new theoretical and observational studies of the potential vorticity distribution in the main thermocline, which provide new tools for interpreting many puzzling features found in the earlier numerical studies. Another motivation is to lay the groundwork for more ambitious numerical models which will penetrate into the parameter range in which mesoscale eddies are dominant in regions of intense currents.

Analytic studies of the thermocline must be highly idealized, if they are to be easily understood. Thus, it is not easy to visualize the relation between the Rhines and Young theories, based on quasi-geostrophic models, and the LPS theory which allows potential vorticity to be injected into the thermocline from outcrops. It is even more difficult to understand all the connections of these theories with McCartney's observational studies of convectively-generated mode waters. In principle, the model used in this study is general enough to include all the mechanisms discussed by these authors, although by restricting the model to steady state solutions we have been confined to a somewhat diffusive region of parameter space. The role of convection in the poleward part of ocean basins is analogous to its role in the tropical atmosphere. In both cases it is of fundamental importance to the general circulation. Convection is excluded *a priori* in a quasi-geostrophic model. However, the more general model used in this study is able to demonstrate how potential vorticity, created by surface heating and Ekman pumping at low latitudes, is transported to higher latitudes and destroyed by convection. In the absence of winds, the low potential vorticity water thus formed sinks to the deep ocean and creates the relatively homogeneous mass of water underlying the thermocline at all latitudes. When winds are added, the poleward edge of the wind generated subtropical gyre intersects the convective region, causing a portion of the convectively generated low potential vorticity water to be diverted from its path to the deep ocean. Instead, this water is advected equatorward within the gyre and injected into the thermocline. Thus, distinctive mode waters are formed within the thermocline by the combined action of surface buoyancy-flux-producing convection and wind driving. The geometry of the trajectories which inject the mode waters into the thermocline is, in agreement with McCartney's (1982) observations, such that progressively deeper density layers receive mode waters across the basin from west to east. Seasonal effects are not found to be essential in the process of mode water formation in the model, although they clearly have a strong modulating effect in the real ocean.

The trajectories of particles in the interior of the subtropical gyre do not extend far enough poleward to be affected by convection. This inner part of the gyre is analogous to the "pool" region of LPS, where the outer part of the gyre corresponds to their "ventilated" region. "Ventilation ages," computed in the model as the elapsed time since a particle has been exposed to surface conditions, show a delineation between these two regions, with a third, unventilated region equatorward of the subtropical gyre corresponding to the "shadow" zone of LPS. A great difference in ventilation age exists across the boundary between the ventilated region and the shadow region, in agreement with the tritium observations of Broecker *et al.* (1978). However, a much smaller age contrast is seen between the pool region and the ventilated region. Instead of exhibiting closed trajectories, as in the idealized theory of Rhines and Young (1982), the particles in the pool region move on downward spirals, undergoing strong mixing within the western boundary current. This diffusively aided ventilation process approaches the efficiency of the purely advective ventilation of the "ventilated" region, resulting in only moderate age contrast between the two regions. This absence of contrast is in agreement with the tritium observations of Sarmiento (1983).

Acknowledgments. The authors would like to thank Joe Pedlosky, Peter Rhines and Jorge Sarmiento for helpful discussions and suggestions. We are also grateful to Betty Williams, Joan Pege and Phil Tunison for assistance in preparing the manuscript.

REFERENCES

Broecker, W. S., T-H. Peng and M. Stuiver, 1978: An estimate of the upwelling rate in the equatorial Atlantic based on the distribution of bomb radiocarbon. *J. Geophys. Res.*, **83**, 6179–6186.

Bryan, K., 1969: A numerical method for the study of the circulation of the World Ocean. *J. Comput. Phys.*, **4**, 347–376.

——, 1984: Accelerating the convergence to equilibrium of ocean-climate models. *J. Phys. Oceanogr.*, **14**, 666–673.

——, and M. D. Cox, 1968: A nonlinear model of an ocean driven by wind and differential heating. Part 1: Description of the three-dimensional velocity and density fields. *J. Atmos. Sci.*, **25**, 945–967.

Gordon, A. L., 1981: South Atlantic thermocline ventilation. *Deep-Sea Res.*, **28A**, 1239–1264.

Haney, R. L., 1971: Surface thermal boundary condition for ocean circulation models. *J. Phys. Oceanogr.*, **1**, 241–248.

Holland, W. R., 1971: Ocean tracer distributions. Part 1: A preliminary numerical experiment. *Tellus*, **23**, 371–392.

——, T. Keffer and P. B. Rhines, 1984: The dynamics of the oceanic general circulation: The potential vorticity field. Submitted to *Nature*.

Ierley, G. R., and W. R. Young, 1983: Can the western boundary layer affect the potential vorticity distribution in the Sverdrup interior of a wind gyre? *J. Phys. Oceanogr.*, **13**, 1753–1763.

Luyten, J. R., J. Pedlosky and H. Stommel, 1983: The ventilated thermocline. *J. Phys. Oceanogr.*, **13**, 292–309.

McCartney, M. S., 1982: The subtropical recirculation of mode waters. *J. Mar. Res.*, **40**(Suppl.), 427–464.

——, L. V. Worthington and M. E. Raymer, 1980: Anomalous water mass distributions at 55°W in the North Atlantic in 1977. *J. Mar. Res.*, **38**, 147–172.

McDowell, S., P. B. Rhines and T. Keffer, 1982: North Atlantic potential vorticity and its relation to the general circulation. *J. Phys. Oceanogr.*, **12**, 1417–1436.

Pedlosky, J., 1984: Eastern boundary ventilation and the structure of the thermocline. *J. Phys. Oceanogr.*, **13**, 2038–2044.

Rhines, P. B., and W. Young, 1982: A theory of wind-driven ocean circulation, I. Mid-ocean gyres. *J. Mar. Res.*, **40**(Suppl.), 559–596.

Robinson, M. K., R. A. Bauer and E. H. Schroeder, 1979: *Atlas of North Atlantic–Indian Ocean Monthly Mean Temperature and Mean Salinities of the Surface Layer.* Naval Oceanographic Office, Bay St. Louis, MS, 213 pp.

Sarmiento, J. L., 1983: A tritium box model of the North Atlantic thermocline. *J. Phys. Oceanogr.*, **13**, 1269–1274.